THE JOURNAL OF PHYSICAL CHEMISTRY LETTERS
A JOURNAL OF THE AMERICAN CHEMICAL SOCIETY

pubs.acs.org/JPCL

Letter

Visualizing the Hierarchical Evolution of Aryl–Metal Bonding in Organometallic Nanostructures on Ag(111)

Yuhong Gao,[†] Zhaoyu Zhang,[†] Zewei Yi, Chi Zhang,* and Wei Xu*

Cite This: *J. Phys. Chem. Lett.* 2023, 14, 10819–10824

Read Online

ACCESS | Metrics & More | Article Recommendations | Supporting Information

ABSTRACT: On-surface dehalogenative coupling reactions are promising for constructing nanostructures with diverse properties and functionalities. Extensive efforts have been devoted to single aryl–halogen (C–X) substituents and substitutions at various functionalization sites (typically including *meta*- and *para*-substitutions) to generate aryl–aryl single bonds. Moreover, multiple C–X substituents at the *ortho*-site and the *peri*- and *bay*-regions have been applied to create a variety of ring scaffolds. However, for multiple C–X substituents, the hierarchy of aryl–metal bond formation and dissociation remains elusive. Herein, by combining scanning tunneling microscopy imaging and density functional theory calculations, we have visualized and demonstrated the hierarchical evolution of aryl–metal bonding in organometallic intermediates involved in a dehalogenative coupling reaction on Ag(111), using a molecular precursor with both *para*-substitution and potential *bay*-region substitution. Our results elucidate how metal atoms are progressively embedded into and removed from organometallic intermediates, enhancing the understanding of on-surface dehalogenative coupling reactions for the controlled construction of the desired nanostructures.

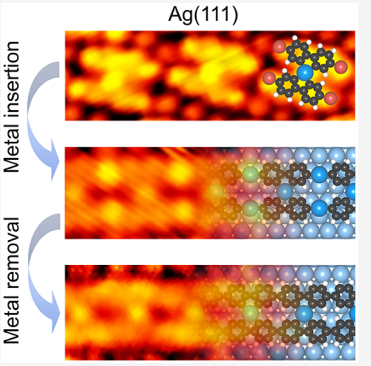

Programmable construction of carbon-based nanostructures holds great promise for the controllable fabrication of molecular electronics.[1] The pioneering work of Grill et al.[2,3] has established on-surface synthesis as a versatile strategy for the bottom-up fabrication of diverse molecule-based nanostructures in desired patterns with atomic precision, encompassing a wide range of C–X (X presents halogen) and C–H activation and C–C coupling reactions.[4,5] Among others, the dehalogenative coupling reaction stands out as one of the most widely applied reactions featured by a well-controlled reaction manner. In this regime, traditional Ullmann coupling reactions with multiple aryl–halogen (including I, Br, and Cl) substituents allow for the hierarchical growth of nanostructures. Moreover, various functionalization sites other than single C–X substituents[6,7] have been extensively introduced, including *meta*-[8] and *para*-substitutions[9] (see more details in Figure S1) to form aryl–aryl single bonds. As an extension, dehalogenative cyclization has been further realized based on more complicated *ortho*-dihalo substitutions (Figure S1), resulting in the generation of four- and six-membered ring scaffolds.[10−13] In addition, *peri*-region[14,15] and *bay*-region[16−19] substitutions (Figure S1) as well as their combination[20] have been exploited and validated to be useful in producing a variety of ring structures, including six-, eight-, and four-membered ones, respectively, further enriching the toolbox for generating *n*-membered nonbenzenoid rings with fascinating properties embedded. Specifically, due to the complexity of multiple C–X activation,[21] a single-sided *bay*-region substitution was shown to be distinct from the double-sided ones[17] in both reaction pathways and products. For the combination of *peri*- and *bay*-region substitutions, various organometallic intermediates produced in the evolution process have been visualized[20] to track the reaction pathways. However, as for the case of multiple aryl–halogen substituents, the hierarchy of multiple aryl–metal formation and dissociation is still elusive. Therefore, it is of general interest to visualize the hierarchical evolution of aryl–metal bonding in organometallic nanostructures in real space, which is crucial for understanding complicated dehalogenative coupling reactions with multiple aryl–halogen substituents.

In this work, the hierarchical evolution of aryl–metal bonding in organometallic nanostructures, including both metalation and demetalation, was visualized in a stepwise manner on Ag(111). The molecular precursor, 4,4′-dibromo-2,2′-diiodo-1,1′-biphenyl (abbreviated as DBIBP) molecule, was selected, consisting of *para*-substitution and potential *bay*-region substitution of C–X bonds (cf. Scheme 1). By a combination of high-resolution scanning tunneling microscopy (STM) imaging and density functional theory (DFT) calculations, we show a hierarchical dehalogenative coupling reaction of DBIBP molecules, including sequential *bay*-metal and *para*-metal insertion and their removal in reverse order,

Received: October 22, 2023
Revised: November 22, 2023
Accepted: November 27, 2023

https://doi.org/10.1021/acs.jpclett.3c02950
J. Phys. Chem. Lett. 2023, 14, 10819–10824

Scheme 1. Reaction Pathways of DBIBP Molecules on Ag(111), Involving the Hierarchical Evolution of Organometallic Intermediates toward the Construction of Aryl−Aryl Coupled Carbon-Based Nanochains

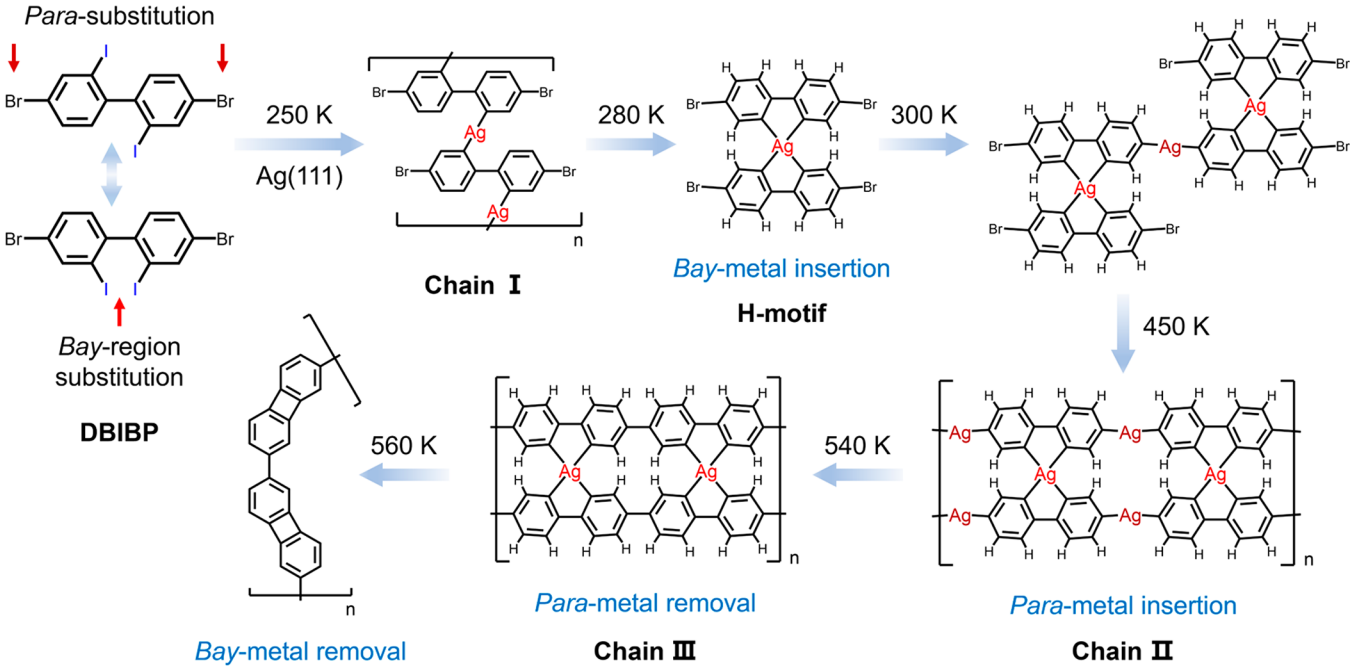

leading to the generation of aryl−aryl coupled carbon-based nanochains consisting of four-membered ring structures. Upon deposition of DBIBP on Ag(111) at ∼250 K, singly bonded organometallic chains (designated as chains I, cf. Scheme 1) were initially formed via C−I activation, followed by dimerization, leading to the formation of H-shaped motifs (shortened as H-motifs) via *bay*-Ag insertion. Subsequently, further C−Br activation at the *para*-sites was gradually induced above room temperature (RT, ∼300 K), forming staggered organometallic oligomers and chains via C−Ag−C bonds on one side of the H-motifs, until the complete *para*-Ag insertion on both sides, which was accompanied by the formation of elongated, ladder-like chains (chains II, cf. Scheme 1). Further elevated temperatures led to the structural transformations with the *para*-Ag removal (forming chains III, cf. Scheme 1), followed by the *bay*-Ag removal, and eventually resulted in the construction of aryl−aryl coupled carbon-based nanochains. Based on the model system containing multiple C−X substituents, this study elucidates how the metal atoms are progressively embedded into and removed from the organometallic intermediates, thereby providing fundamental insights into on-surface dehalogenative reactions for the controlled construction of desired nanostructures.

Upon deposition of DBIBP molecules on Ag(111) held at ∼250 K, large islands composed of long chains were constructed (Figure 1a). The magnified STM image (Figure 1b) shows that these chains (chains I, cf. Scheme 1) consist of parallel short rods that are interconnected by bright dots located at the central region of both sides, thereby facilitating outward expansion, and are separated by dark dots (as typically depicted by green circles) between neighboring chains. Considering the cleavage of C−I bonds at lower than 200 K on Ag(111) followed by the insertion of Ag adatoms,[22,23] we proposed that chain I was formed by deiodinated *trans*-DBIBP molecules linked by Ag adatoms and was surrounded by dissociated iodine atoms.[18] To corroborate this hypothesis,

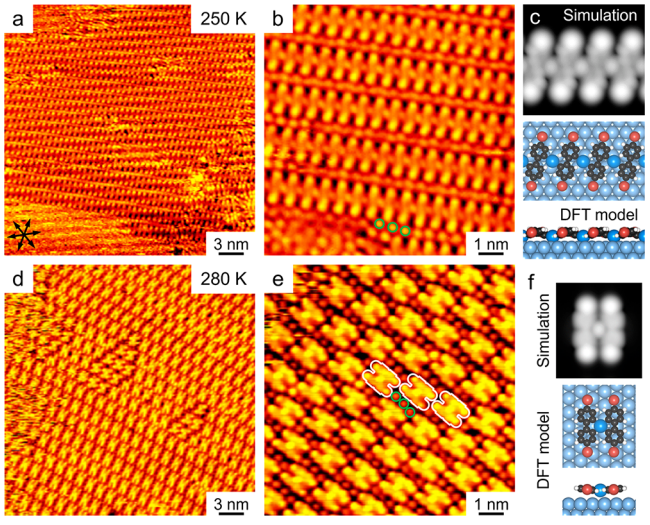

Figure 1. Formation of chains I and H-motifs on Ag(111). (a) Large-scale and (b) magnified STM images showing the formation of chains I surrounded by dissociated iodine atoms (highlighted in green circles) after deposition of DBIBP molecules on Ag(111) held at ∼250 K. (c) STM simulation and corresponding DFT-optimized structural model of chain I on Ag(111). (d) Large-scale and (e) magnified STM images showing the appearance of H-motifs at ∼280 K, with individual H-motifs typically depicted by white contours. (f) STM simulation and corresponding DFT-optimized structural model of the H-motif on Ag(111). Scanning conditions: $V = -1.2$ V, $I = 0.6$ nA. The close-packed directions of the Ag(111) substrate are indicated by the black arrows. Ag substrate: light blue; Ag adatom: navy blue; C: gray; H: white; Br: brown.

DFT calculations were performed on the chain structure. The DFT-optimized structural model displays that the deiodinated DBIBP monomers interconnect with each other through free Ag adatoms in a *trans*-configuration, leading to the formation of C−Ag−C bonds on both sides (lower panel of Figure 1c).

https://doi.org/10.1021/acs.jpclett.3c02950
J. Phys. Chem. Lett. 2023, 14, 10819−10824

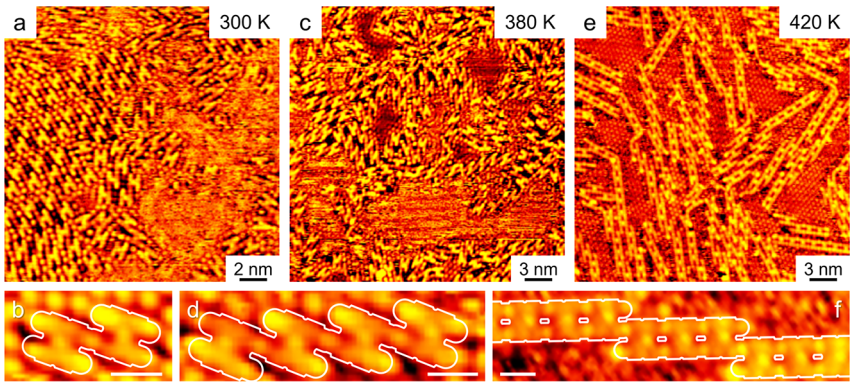

Figure 2. Stepwise growth from H-motifs to H-based organometallic chains via aryl−Ag bonding at the *para*-sites on Ag(111). (a) High-resolution STM image of organometallic oligomers and (b) enlarged STM image of a typical H-based organometallic dimer obtained at ∼300 K. (c) Large-scale STM image showing the formation of longer organometallic oligomers after annealing at ∼380 K. (d) A typical organometallic oligomer with "single-leg" coupled via *para*-Ag insertion. (e) Large-scale STM image of organometallic chains with more *para*-Ag atoms inserted after annealing at ∼420 K. (f) Magnified STM image of a typical organometallic chain. Scale bars in (b, d, f): 1 nm. Scanning conditions: $V = -1.2$ V, $I = 0.6$ nA.

Due to the lower adsorption height of Ag adatoms, the aryl groups directly bonded to the Ag adatoms are bent down toward the surface on the interacting sides, while the other sides are tilted away from the surface (see the side view of the model). The corresponding STM simulation (top panel of Figure 1c) thus allows us to attribute the sinuous rods and the two bright dots at each end of the rods to the biphenyl moieties with a nonplanar configuration and the attached Br atoms, respectively. The Ag adatoms between two neighboring molecular components appear as dots, which is in good agreement with the experimental observations.

Subsequently, the sample was annealed at ∼280 K, and self-assembled islands composed of H-motifs were formed (Figure 1d). The zoomed-in STM image (Figure 1e) shows more details of these islands, where H-motifs (highlighted in white contours) are surrounded by iodine dots (in green circles) and alternately packed into molecular islands. Each H-motif consists of two bent rods with a bright dot attached to each end, referred to as two "legs", while a large bright dot is located at the center connecting the two legs. Based on the morphology and dimension shown in the submolecularly resolved STM image, the two bent legs and the interlinked bright dots are suggested to be the deiodinated DBIBP components in a *cis*-configuration and the central Ag adatoms, respectively. Then, DFT calculations were carried out on the H-motif. The DFT-optimized model verifies that the two deiodinated *cis*-DBIBP components are linked via a Ag adatom forming 4-fold C−Ag bonds in the *bay*-region[18,19] and are thus less tilted compared to the situation of *trans*-DBIBP (as shown in Figure 1c), while four Br substituents remain at the ends (Figure 1f). The corresponding STM simulation agrees well with the experimental one, further confirming the above scenario. Thus, in the step between chains I and H-motifs, the C−Ag−C bonds in chains I were partially cleaved due to the dynamic features of such organometallic bonds,[24] accompanied by the flipping of bromobenzene moieties along the C_{aryl}−C_{aryl} single bonds, resulting in the formation of H-motifs with four C−Ag bonds holding a Ag adatom in the *bay*-region. Such a structural transformation also indicates that the *bay*-metal insertion (in a *cis*-configuration) is energetically more favorable on Ag(111).

As the metal insertion via C−Br cleavage requires elevated temperatures, the above sample was further annealed at ∼300 K, and the self-assembled structures of H-motifs became less ordered with the majority of the H-motifs coupled via the connection of one "leg" to form staggered oligomers with different numbers of units involved (Figure 2a). A typical H-based organometallic dimer structure is illustrated in Figure 2b, where two H-motifs are connected together by sharing one bright dot at the junction, suggesting the occurrence of C−Br bonds cleavage and Ag adatom insertion to form C−Ag−C bonds.[11,21,25] Upon further annealing at ∼380 K, longer organometallic oligomers emerged (Figure 2c). A close inspection of a typical H-based organometallic oligomer shows that it is composed of several H-motifs connected by Ag adatoms through "single-legs" (Figure 2d). Increasing the annealing temperature to ∼420 K further led to the construction of long ladder-like chain structures (chains II, cf. Scheme 1) with an increasing number of dissociated halogen atoms filling in the free space around the nanostructures (Figure 2e), indicating the cleavage of more C−Br bonds in this state. It is also worth noting that a few "single-leg" coupled oligomers are also visible at the junctions, as shown in the center of Figure 2e, and the chain structures are less ordered. The close-up STM image of a representative organometallic chain is shown in Figure 2f, where both "single-leg" and "two-leg" coupled fragments are present and interconnected. In the "two-leg" coupled parts, the H-motifs are completely debrominated on both ends and connected by two bright dots (which are attributed to Ag adatoms) via C−Ag−C bonds (which will be discussed in detail below) as reported in a similar situation.[20,25] At the same time, due to incomplete C−Br cleavage, some "two-leg" coupled fragments were linked together by single C−Ag−C bonds, forming extended chains. Note that the reaction barriers of C−I and C−Br activation on Ag(111) were theoretically reported to be 0.81 and 0.52 eV,[26] respectively, and previous experimental results reported that complete C−Br activation took place at above 125 °C, while the C−I activation usually occurred below RT on Ag(111),[23,27] which are in good agreement with our experimental observations. Therefore, at this stage, hierarchical metal insertion stemming from C−I and C−Br activation has been experimentally visualized on Ag(111), with *bay*-Ag and *para*-Ag atoms progressively inserted into nanostructures, resulting in the propagation of organometallic chains.

To induce the complete *para*-metal insertion, the above sample was further annealed to a higher temperature of ∼450 K. As a result, more well-ordered and longer ladder-like

https://doi.org/10.1021/acs.jpclett.3c02950
J. Phys. Chem. Lett. 2023, 14, 10819−10824

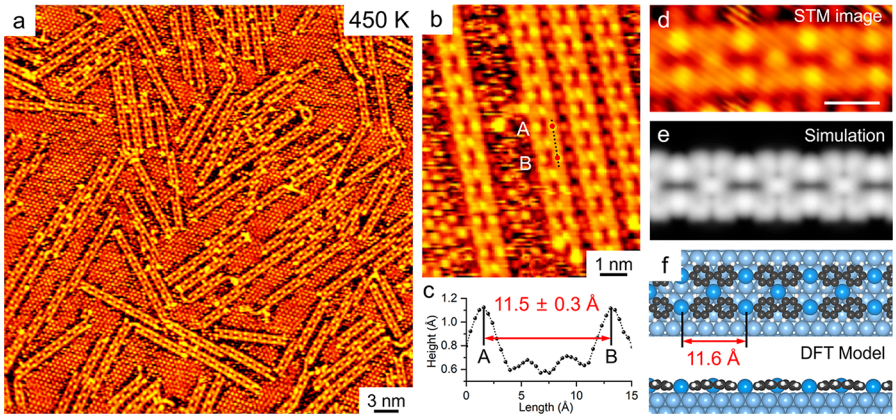

Figure 3. Construction of ladder-like organometallic chains (chains II) on Ag(111) with both *bay*-metals and *para*-metals inserted. (a) Large-scale and (b) close-up STM images showing the formation of chains II after annealing at ∼450 K. (c) Line profile along the black dotted line in (b). (d) Zoomed-in STM image of chain II, (e) simulated STM image, and (f) DFT-optimized structural models in top and side views. Ag substrate: light blue; Ag adatom: navy blue; C: gray; H: white; Br: brown. Scanning parameters: $V = -1.2$ V, $I = 0.6$ nA.

organometallic chains (chains II) were prepared on Ag(111), while more halogen atoms were dissociated from the molecules and occupied the remaining regions (Figure 3a). Simultaneously, fewer "single-leg" coupled junctions were found, which is an indication of further completion of the *para*-metal insertion. From the zoomed-in high-resolution STM image of chain II (Figure 3b,d), it can be clearly identified that H-motifs connect with each other by sharing two bright dots at the junctions in a "two-leg"-coupling mode, extending to form long ladder-like chains. According to the scenario discussed above and the previous reports,[20,25,28] the bright dots are attributed to the embedded Ag atoms. In addition, the periodicity of such a chain (which is indicated by the red dots denoted as A and B in Figure 3b) was experimentally measured to be 11.5 ± 0.3 Å, as shown in the line profile in Figure 3c. To further corroborate the organometallic structure, the corresponding DFT calculations on chain II were performed. The DFT-optimized model confirmed that H-motifs constructed organometallic chains through C−Ag−C bonds on both sides (Figure 3f), where the distance between two neighboring *para*-Ag atoms was calculated to be 11.6 Å, in good agreement with the experimental result (Figure 3c). Moreover, the corresponding STM simulation (Figure 3e) successfully reproduced the STM morphology, further validating the involvement of both *bay*-metals and *para*-metals (appearing as bright dots) in the structure of chain II. In this way, after the C−X activation of the *bay*-region diiodo-substitution and *para*-bromo-substitution in a progressive manner, Ag adatoms have been hierarchically inserted to form multiple aryl−Ag bonds, eventually constructing the ladder-like organometallic chains, while all the halogens in DBIBP molecules have been dissociated.

In an attempt to further elucidate the demetalation process, the annealing temperature was further increased to induce the cleavage of multiple aryl−Ag bonds within the organometallic intermediates and subsequent coupling process on Ag(111).[25,29] After annealing at ∼540 K, a new type of ladder-like H-based organometallic chains (referred to as chains III and highlighted by the blue rectangle, cf. Scheme 1) appeared, coexisting with some remaining fragments of chain II (Figure 4a). Notably, compared to chain II, the bright dots of *para*-Ag connecting H-based components disappeared in chain III, suggesting the removal of *para*-Ag atoms at these sites,

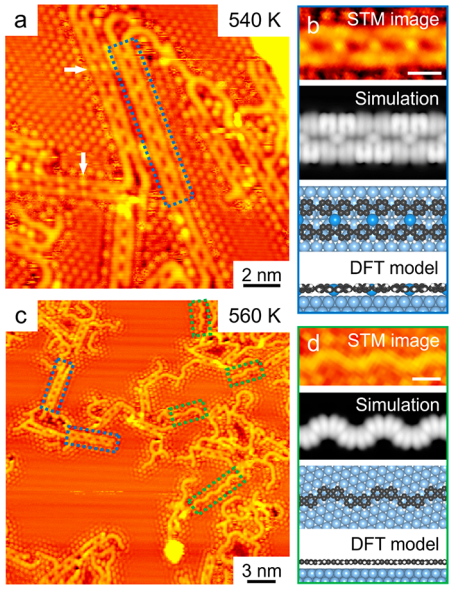

Figure 4. Hierarchical aryl-metal removal and subsequent C−C coupling processes. (a) High-resolution STM image showing the formation of chains III at ∼540 K, as typically indicated by the blue dashed rectangle, with the coexistence of some remaining *para*-Ag atoms in the chains (indicated by white arrows). (b) Submolecularly resolved STM image, STM simulation, and top and side views of the DFT-optimized structural model of chain III on Ag(111). (c) STM image showing the coexistence of C−C coupled chains and chain III after further annealing at ∼560 K, as indicated by green and blue rectangles, respectively. (d) STM image of a C−C coupled chain, corresponding STM simulation, and DFT-optimized structural model in top and side views. Scale bars in (b, d): 1 nm. Ag substrate: light blue; Ag adatom: navy blue; C: gray; H: white; Br: brown. Scanning parameter: $V = -1.2$ V, $I = 0.6$ nA.

while some still survived in other chains as typically indicated by the white arrows. Such an obvious contrast in the STM topography indicates that the aryl−Ag cleavage and C−C coupling reaction at the *para*-sites have occurred but are incomplete. On the contrary, the *bay*-Ag atoms are still present in chains III. In addition, the submolecularly resolved STM image of chain III (top panel of Figure 4b) clearly displays a distinct apparent contrast, with adjacent "legs" of H-based molecular components exhibiting alternating brightness on the

https://doi.org/10.1021/acs.jpclett.3c02950
J. Phys. Chem. Lett. 2023, 14, 10819−10824

same and opposite sides, which greatly differs from that of chain II with a uniform contrast. Accordingly, DFT calculations were carried out, and the DFT-optimized model (bottom panel of Figure 4b) shows the direct C−C coupling between adjacent debrominated H-based components, with the *bay*-Ag atoms inserted but the *para*-Ag atoms removed. Due to the steric hindrance among four adjacent hydrogen atoms in the cavity,[28] the biphenyl moieties adopt an alternately tilted configuration as shown in the side view, leading to the zigzag topography and the apparent contrast in the corresponding STM simulation (middle of Figure 4b). Thus, the simulated STM image shows a nice agreement with the experimental one as well as with the situation described in the recent work.[28] Moreover, the structural model in an almost planar configuration without alternate tilting (Figure S2) was also constructed and calculated to be energetically less stable by 0.16 eV. The corresponding STM simulation displays uniform brightness with no apparent contrast in the biphenyl moieties (Figure S2), further supporting the above hypothesis. In addition, the binding energies of C−Ag bonding were calculated to be −8.33 and −5.57 eV per Ag adatom at the *bay*-region and the *para*-site (Figure S3), respectively, indicating the higher stability of the *bay*-metal connection than that of *para*-metal from the viewpoint of thermodynamics. In this way, *para*-Ag removal was achieved with the increased annealing temperature, showing the relative weakness of the C−Ag−C bond at the *para*-site compared to that at the *bay*-region.

As the next step, the sample was heated to ∼560 K to induce further demetalation, which resulted in the appearance of disordered single-strand curved chains in the majority as typically highlighted by the green rectangles in Figure 4c. At the same time, some chains III are also preserved (indicated by the blue rectangles). The close-up STM image of a typical curved chain (top panel of Figure 4d) shows that the width is similar to that of a single "leg" in the H-based chains (chains II and III), indicating the removal of *bay*-Ag atoms in this structure. Accordingly, further C−C coupling at the *bay*-region could be induced to form four-membered rings, as observed in the previous work.[19] Following such a speculation, the structural model was optimized and shows that after the removal of *bay*-Ag atoms and C−C coupling, a four-membered ring is generated, eventually leading to the synthesis of 646-ringed units connected together by C−C single bonds (bottom panel of Figure 4d). The characteristic curved structures also rationalize the formation of the four-membered rings in the majority, which are well-reproduced in the simulated STM image (middle of Figure 4d), with the chain appearing as a thin stripe with uniform brightness. Nevertheless, due to the complexity of multiple active sites at higher temperatures, side reactions may also be triggered, and no well-ordered chains could be obtained. Therefore, we have shown that *para*-metal and *bay*-metal atoms are removed from organometallic intermediates in a hierarchical manner, with the sequence reversed compared to that of the metal insertion process.

In conclusion, by combining STM imaging and DFT calculations, we have visualized and demonstrated the hierarchical evolution of aryl−metal bonding in organometallic intermediates involved in a dehalogenative coupling reaction on Ag(111), which is based on molecular modification with both *para*-substitution and potential *bay*-region substitution. Following a stepwise annealing strategy, both the insertion of *bay*-metal and *para*-metal atoms and their removal in reverse order were captured experimentally, accompanied by the generation and transformation of organometallic intermediates, which were further theoretically verified by DFT calculations. Our findings have the potential to provide fundamental understandings of on-surface dehalogenative coupling reactions with multiple aryl−halogen substituents and to further broaden their applications for the controlled construction of desired nanostructures with atomic precision.

■ ASSOCIATED CONTENT

Supporting Information

The Supporting Information is available free of charge at https://pubs.acs.org/doi/10.1021/acs.jpclett.3c02950.

Experimental methods, details of DFT calculations, and additional calculated structures and binding energies (PDF)

■ AUTHOR INFORMATION

Corresponding Authors

Chi Zhang − *Interdisciplinary Materials Research Center, School of Materials Science and Engineering, Tongji University, Shanghai 201804, People's Republic of China*; Email: zhangchi11@tongji.edu.cn

Wei Xu − *Interdisciplinary Materials Research Center, School of Materials Science and Engineering, Tongji University, Shanghai 201804, People's Republic of China*; orcid.org/0000-0003-0216-794X; Email: xuwei@tongji.edu.cn

Authors

Yuhong Gao − *Interdisciplinary Materials Research Center, School of Materials Science and Engineering, Tongji University, Shanghai 201804, People's Republic of China*

Zhaoyu Zhang − *Interdisciplinary Materials Research Center, School of Materials Science and Engineering, Tongji University, Shanghai 201804, People's Republic of China*

Zewei Yi − *Interdisciplinary Materials Research Center, School of Materials Science and Engineering, Tongji University, Shanghai 201804, People's Republic of China*

Complete contact information is available at: https://pubs.acs.org/10.1021/acs.jpclett.3c02950

Author Contributions

†These authors contribute equally.

Notes

The authors declare no competing financial interest.

■ ACKNOWLEDGMENTS

The authors acknowledge financial support from the National Natural Science Foundation of China (Grants Nos. 22202153, 22125203, and 21790351), the Fundamental Research Funds for the Central Universities, and Ministry of Science and Technology of the People's Republic of China (2023YFE-0101900). The authors are grateful for the use of RIKEN's HOKUSAI supercomputer system.

■ REFERENCES

(1) Yin, J.; Jacobse, P. H.; Pyle, D.; Wang, Z.; Crommie, M. F.; Dong, G. Programmable Fabrication of Monodisperse Graphene Nanoribbons via Deterministic Iterative Synthesis. *J. Am. Chem. Soc.* **2022**, *144*, 16012−16019.

(2) Grill, L.; Dyer, M.; Lafferentz, L.; Persson, M.; Peters, M. V.; Hecht, S. Nano-Architectures by Covalent Assembly of Molecular Building Blocks. *Nat. Nanotechnol.* **2007**, *2*, 687−691.

(3) Lafferentz, L.; Eberhardt, V.; Dri, C.; Africh, C.; Comelli, G.; Esch, F.; Hecht, S.; Grill, L. Controlling On-Surface Polymerization by Hierarchical and Substrate-Directed Growth. *Nat. Chem.* **2012**, *4*, 215−220.
(4) Grill, L.; Hecht, S. Covalent On-Surface Polymerization. *Nat. Chem.* **2020**, *12*, 115−130.
(5) Zhang, C.; Yi, Z.; Xu, W. Scanning Probe Microscopy in Probing Low-Dimensional Carbon-Based Nanostructures and Nanomaterials. *Mater. Futures* **2022**, *1*, No. 032301.
(6) Zhou, X.; Wang, C.; Zhang, Y.; Cheng, F.; He, Y.; Shen, Q.; Shang, J.; Shao, X.; Ji, W.; Chen, W.; et al. Steering Surface Reaction Dynamics with a Self-Assembly Strategy: Ullmann Coupling on Metal Surfaces. *Angew. Chem., Int. Ed.* **2017**, *56*, 12852−12856.
(7) Zint, S.; Ebeling, D.; Schlöder, T.; Ahles, S.; Mollenhauer, D.; Wegner, H. A.; Schirmeisen, A. Imaging Successive Intermediate States of the On-Surface Ullmann Reaction on Cu(111): Role of the Metal Coordination. *ACS Nano* **2017**, *11*, 4183−4190.
(8) Eichhorn, J.; Nieckarz, D.; Ochs, O.; Samanta, D.; Schmittel, M.; Szabelski, P. J.; Lackinger, M. On-Surface Ullmann Cupling: the Influence of Kinetic Reaction Parameters on the Morphology and Quality of Covalent Networks. *ACS Nano* **2014**, *8*, 7880−7889.
(9) Wang, W.; Shi, X.; Wang, S.; Van Hove, M. A.; Lin, N. Single-Molecule Resolution of an Organometallic Intermediate in a Surface-Supported Ullmann Coupling Reaction. *J. Am. Chem. Soc.* **2011**, *133*, 13264−13267.
(10) Sánchez-Sánchez, C.; Nicolaï, A.; Rossel, F.; Cai, J.; Liu, J.; Feng, X.; Müllen, K.; Ruffieux, P.; Fasel, R.; Meunier, V. On-Surface Cyclization of ortho-Dihalotetracenes to Four- and Six-Membered Rings. *J. Am. Chem. Soc.* **2017**, *139*, 17617−17623.
(11) Zhang, C.; Kazuma, E.; Kim, Y. Atomic-Scale Visualization of the Stepwise Metal-Mediated Dehalogenative Cycloaddition Reaction Pathways: Competition between Radicals and Organometallic Intermediates. *Angew. Chem., Int. Ed.* **2019**, *58*, 17736−17744.
(12) Zhang, R.; Xia, B.; Xu, H.; Lin, N. Identifying Multinuclear Organometallic Intermediates in On-Surface [2 + 2] Cycloaddition Reactions. *Angew. Chem., Int. Ed.* **2019**, *58*, 16485−16489.
(13) Li, D.-Y.; Qiu, X.; Li, S.-W.; Ren, Y.-T.; Zhu, Y.-C.; Shu, C.-H.; Hou, X.-Y.; Liu, M.; Shi, X.-Q.; Qiu, X.; Liu, P.-N. Ladder Phenylenes Synthesized on Au(111) Surface via Selective [2 + 2] Cycloaddition. *J. Am. Chem. Soc.* **2021**, *143*, 12955−12960.
(14) Zhang, H.; Lin, H.; Sun, K.; Chen, L.; Zagranyarski, Y.; Aghdassi, N.; Duhm, S.; Li, Q.; Zhong, D.; Li, Y.; et al. On-Surface Synthesis of Rylene-Type Graphene Nanoribbons. *J. Am. Chem. Soc.* **2015**, *137*, 4022−4025.
(15) Zuzak, R.; Brandimarte, P.; Olszowski, P.; Izydorczyk, I.; Markoulides, M.; Such, B.; Kolmer, M.; Szymonski, M.; Garcia-Lekue, A.; Sánchez-Portal, D.; et al. On-Surface Synthesis of Chlorinated Narrow Graphene Nanoribbon Organometallic Hybrids. *J. Phys. Chem. Lett.* **2020**, *11*, 10290−10297.
(16) Liu, M.; Liu, M.; She, L.; Zha, Z.; Pan, J.; Li, S.; Li, T.; He, Y.; Cai, Z.; Wang, J.; et al. Graphene-Like Nanoribbons Periodically Embedded with Four- and Eight-Membered Rings. *Nat. Commun.* **2017**, *8*, 14924.
(17) Zeng, Z.; Guo, D.; Wang, T.; Chen, Q.; Matěj, A.; Huang, J.; Han, D.; Xu, Q.; Zhao, A.; Jelínek, P.; et al. Chemisorption-Induced Formation of Biphenylene Dimer on Ag(111). *J. Am. Chem. Soc.* **2022**, *144*, 723−732.
(18) Feng, L.; Wang, T.; Jia, H.; Huang, J.; Han, D.; Zhang, W.; Ding, H.; Xu, Q.; Du, P.; Zhu, J. On-Surface Synthesis of Planar Acenes via Regioselective Aryl-Aryl Coupling. *Chem. Commun.* **2020**, *56*, 4890−4893.
(19) Kawai, S.; Takahashi, K.; Ito, S.; Pawlak, R.; Meier, T.; Spijker, P.; Canova, F. F.; Tracey, J.; Nozaki, K.; Foster, A. S.; Meyer, E. Competing Annulene and Radialene Structures in a Single Anti-Aromatic Molecule Studied by High-Resolution Atomic Force Microscopy. *ACS Nano* **2017**, *11*, 8122−8130.
(20) Zhong, Q.; Niu, K.; Chen, L.; Zhang, H.; Ebeling, D.; Björk, J.; Müllen, K.; Schirmeisen, A.; Chi, L. Substrate-Modulated Synthesis of Metal-Organic Hybrids by Tunable Multiple Aryl-Metal Bonds. *J. Am. Chem. Soc.* **2022**, *144*, 8214−8222.
(21) Shang, L.; Gao, W.; Kang, F.; Zhang, Z.; Zhang, C.; Xu, W. Real-Space Visualization of Sequential Debromination of Polybrominated Benzenes on Ag(111). *Chem. Commun.* **2023**, *59*, 704−707.
(22) Buelow, M. T.; Gellman, A. J. The Transition State for Metal-Catalyzed Dehalogenation: C−I Bond Cleavage on Ag(111). *J. Am. Chem. Soc.* **2001**, *123*, 1440−1448.
(23) Eichhorn, J.; Strunskus, T.; Rastgoo-Lahrood, A.; Samanta, D.; Schmittel, M.; Lackinger, M. On-Surface Ullmann Polymerization via Intermediate Organometallic Networks on Ag(111). *Chem. Commun.* **2014**, *50*, 7680−7682.
(24) Fan, Q.; Wang, T.; Dai, J.; Kuttner, J.; Hilt, G.; Gottfried, J. M.; Zhu, J. On-Surface Pseudo-High-Dilution Synthesis of Macrocycles: Principle and Mechanism. *ACS Nano* **2017**, *11*, 5070−5079.
(25) Qin, T.; Guo, D.; Xiong, J.; Li, X.; Hu, L.; Yang, W.; Chen, Z.; Wu, Y.; Ding, H.; Hu, J.; et al. Synthesis of a Porous [14]Annulene Graphene Nanoribbon and a Porous [30]Annulene Graphene Nanosheet on Metal Surfaces. *Angew. Chem., Int. Ed.* **2023**, *62*, No. e202306368.
(26) Björk, J.; Hanke, F.; Stafstrom, S. Mechanisms of Halogen-Based Covalent Self-Assembly on Metal Surfaces. *J. Am. Chem. Soc.* **2013**, *135*, 5768−5775.
(27) Bieri, M.; Nguyen, M. T.; Gröning, O.; Cai, J.; Treier, M.; Aït-Mansour, K.; Ruffieux, P.; Pignedoli, C. A.; Passerone, D.; Kastler, M.; et al. Two-Dimensional Polymer Formation on Surfaces: Insight into the Roles of Precursor Mobility and Reactivity. *J. Am. Chem. Soc.* **2010**, *132*, 16669−16676.
(28) Wang, Z.; Yin, R.; Meng, J.; Wang, J.; Liang, Y.; Ma, C.; Tan, S.; Li, Q.; Yang, J.; Wang, B. Self-Limited Embedding Alternating 585-Ringed Divacancies and Metal Atoms into Graphene Nanoribbons. *J. Am. Chem. Soc.* **2023**, *145*, 8445−8454.
(29) Fritton, M.; Duncan, D. A.; Deimel, P. S.; Rastgoo-Lahrood, A.; Allegretti, F.; Barth, J. V.; Heckl, W. M.; Björk, J.; Lackinger, M. The Role of Kinetics versus Thermodynamics in Surface-Assisted Ullmann Coupling on Gold and Silver Surfaces. *J. Am. Chem. Soc.* **2019**, *141*, 4824−4832.

https://doi.org/10.1021/acs.jpclett.3c02950
J. Phys. Chem. Lett. 2023, 14, 10819−10824